minerals

MDPI

Article

Spent NCM Lithium-Ion Batteries: Potential Evaluation of Mechanical Pretreatment for Recycling

Priscila Silva Silveira Camargo *, Maryanne Hoffmann Cardoso, Roberta dos Reis Costantin, Marcelo Pilotto Cenci, Felipe Antonio Lucca Sánchez, Angela Cristina Kasper and Hugo Marcelo Veit *

Laboratory of Corrosion, Protection and Materials Recycling (LACOR), Materials Engineering Department, School of Engineering, Federal University of Rio Grande do Sul (UFRGS), Av. Bento Gonçalves, 9500, Section 4, Building 43426, Porto Alegre 90010-900, Brazil; maryanne.h.cardoso@gmail.com (M.H.C.); robertadosreiscostantin@gmail.com (R.d.R.C.); marcelo.cenci@hotmail.com (M.P.C.); felipe.lucsan@gmail.com (F.A.L.S.); angela.kasper@ufrgs.br (A.C.K.)

* Correspondence: priscila.silveira@ufrgs.br or prisscamargo@gmail.com (P.S.S.C.); hugo.veit@ufrgs.br (H.M.V.)

Abstract: Recent increases in the demand for automotive lithium-ion batteries (LIBs) have led to higher needs for critical materials like lithium, cobalt, nickel, and graphite. Consequently, recovering materials from spent batteries has gained importance. This study aimed to (1) develop a mechanical pretreatment method for separating and concentrating materials from spent NCM_{811} cells and (2) evaluate the economic, environmental, and shortage potentials of these fractions. The pretreatment involved grinding and granulometric separation, producing six particle-size fractions. The main novelty of the study was the assessment to identify the particle size fractions which are priorities for recycling for decision-making by recycling companies, optimizing their resources and efforts. Analysis showed that the finest fraction ($n < 0.5$ mm) had 85% of lithium, 77.4% of cobalt, 75.1% of manganese, and 68.5% of nickel. This fraction represented 40.4% of the processed mass and had the highest economic value (USD 3669/ton NCM cell). This fraction was also prioritized for recycling due to its superior environmental impact (103,788 kg CO_2-eq/ton NCM cell) and scarcity considerations. Furthermore, the black mass of NCM was the priority for recycling and had greater economic, environmental, and supply risk potential than the black mass of LFP cells.

Keywords: spent lithium-ion batteries; NCM cell; recycling; economic potential; environmental impact; shortage of raw materials

Citation: Camargo, P.S.S.; Cardoso, M.H.; Costantin, R.d.R.; Cenci, M.P.; Sánchez, F.A.L.; Kasper, A.C.; Veit, H.M. Spent NCM Lithium-Ion Batteries: Potential Evaluation of Mechanical Pretreatment for Recycling. *Minerals* **2024**, *14*, 1155. https://doi.org/10.3390/min14111155

Academic Editor: Sunil Kumar Tripathy

Received: 15 September 2024
Revised: 7 November 2024
Accepted: 12 November 2024
Published: 15 November 2024

1. Introduction

The demand for automotive lithium-ion batteries (LIBs) increased by about 65% in 2022, driven by the increase in sales of electric vehicles. The outlook is that sales of electric vehicles will continue to increase exponentially in the coming years, mainly in regions such as China, the United States, and Europe, and expand to developing countries [1].

As can be seen in Figure 1, LIBs comprise an anode, a cathode, a separator, electrolytes, and a steel casing. The anode electrode is constituted of a polymer binder and carbon material, such as graphite, and is deposited on a copper sheet. The cathode electrode comprises acetylene black, polymer binder, and lithium transition metal oxides coated on an aluminum sheet. Polyvinylidene fluoride (PVDF), copolymers, and polypropylene (PP) stand out as the predominant binders employed in commercial LIBs. The commonly employed separators encompass microporous polyolefin membranes, including polypropylene (PP), polyethylene (PE), and fluorinated polymers. Meanwhile, diverse LIBs utilize distinct ion electrolytes. For instance, lithium-ion battery electrolytes often feature lithium salts like lithium hexafluorophosphate ($LiPF_6$), lithium tetrafluoroborate ($LiBF_4$), lithium bis(trifluoromethanesulfonyl)imide (LiTFSI), or others, dissolved in polar aprotic alkyl carbonate solvents, such as ethylene carbonate/dimethyl carbonate (EC/DMC) [2].

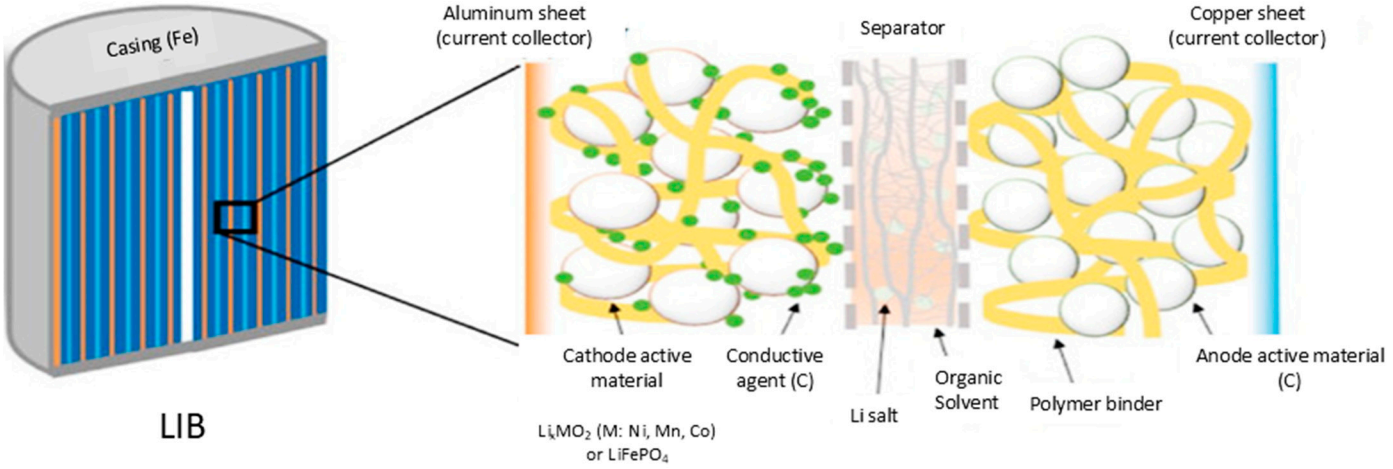

Figure 1. A schematic diagram of the lithium-ion battery components. Source: Adapted from Ji et al., 2021 [3].

Currently, lithium nickel cobalt manganese (NCM) oxide batteries dominate the lithium-ion battery market, with a share of about 60% [1,4]. The NCM term represents a family of cathode active materials used in LIBs with variations stoichiometric in the composition, for example NCM_{111} ($LiNi_{0.33}Co_{0.33}Mn_{0.33}O_2$), NCM_{523} ($LiNi_{0.5}Co_{0.2}Mn_{0.3}O_2$), NCM_{622} ($LiNi_{0.6}Co_{0.2}Mn_{0.2}O_2$), and NCM_{811} ($LiNi_{0.8}Co_{0.1}Mn_{0.1}O_2$). NCM_{111}, containing the same proportions of nickel, manganese, and cobalt, was the first commercially used cathode material, but currently, cathodes containing smaller amounts of cobalt, such as NCM_{622} and NCM_{811}, are increasingly used [1,4,5]. Cations containing a higher nickel ratio present a benefit besides using a lower cobalt ratio and a higher energy density [6,7]. The market share scenario for LIB technologies could change quickly if in the future innovative technologies with superior properties emerge. Trends for the future of battery technologies, with a focus on lithium-based batteries, point to advanced nickel (Ni)-rich NCM batteries (NCM_{811}), lithium–sulfur (Li-S) batteries, solid-state lithium (solid-Li) batteries, and lithium–air (Li-Air) batteries, with emphasis particularly placed on advanced nickel-rich NCM batteries (NCM_{811}) [8,9].

NCM and lithium iron phosphate (LFP) batteries are the most widely used power LIBs in electric vehicles [10]. LFP cells are currently a popular alternative to NCM cells, in which the cathode material has high structural stability, allowing for long service life and being more economical to produce [11,12]. Jiang et al. (2022) found that the production of LFP cells has a lower environmental impact per kilogram compared to NCM cells. This difference is primarily due to the cathode material, which represents over 37%–43% of the manufacturing impacts for LFP cells and around 50% for NCM cells. The precursor for the NCM cathode, which includes metallic compounds such as nickel, manganese, and cobalt, requires more resources and energy to process compared to the iron phosphate precursor used in LFP cathodes, leading to higher environmental impacts during its production [13].

Quan et al. (2022) carried out a comprehensive life-cycle assessment (LCA) comparing LFP and NCM batteries from production to end-of-life. The main conclusions indicate that the production phases of batteries, the initial use for electric vehicles, and secondary use in energy storage systems contribute most significantly to environmental impacts, which can be mitigated through recycling processes, in particular hydrometallurgical methods. The study indicated that LFP batteries have a higher overall environmental impact compared to NCM batteries because the LFP battery, having a lower energy density, required a greater amount of LFP cathode material and additional metals to meet the same performance requirements. The charge–discharge efficiency during the use phases was identified as a crucial factor influencing the environmental performance of both battery types. It is worth noting that these calculations considered China, which has an energy matrix associated

with high carbon emissions, so switching to a renewable energy matrix would reduce these impacts [10].

The increase in demand for automotive LIBs has a direct impact on increasing the demand for critical materials such as lithium, cobalt, nickel, and graphite. This continuous and rapid increase in demand for these materials is a source of concern worldwide. In 2022, for example, the automotive battery industry responded to about 60% of lithium demands, and despite the increase in its production, lithium demand exceeded supplies. As a result, lithium carbonate prices have increased significantly, in such a way that at the beginning of 2023, prices reached levels up to six times above the average prices practiced during the 2015–2020 period [1]. In the cobalt case, increases in prices and the possibility of disruption in mineral supply (about 70% of world cobalt mine production comes from Congo, a region marked by internal conflicts) contributed to the use of cathodes rich in nickel and with lower cobalt content. However, the use of this type of cathode caused an increase in nickel prices in 2022, which reached double the average price in the period 2015–2020. Associated with the price increase, there is a growing concern related to supply risks [1,4,5]. Regarding graphite, another important component, its use in batteries, has grown by 250% since 2018 [5].

Another source of concern is the substantial number of LIBs that will reach their end-of-life (EOL) in the coming years. Inadequate disposal of these spent batteries may cause health and environmental impacts due to the presence of toxic materials in their composition. On the other hand, the spent LIBs could be a source of critical minerals [9,14]. However, the concentration of metals of high economic value present in LIBs depends on the type of battery analyzed. NCM LIBs, for example, contain Li, Co, Ni, Mn, Cu, and graphite in their composition. According to Dunn et al. [15], 11%–12% of cobalt, 7%–8% of lithium, and 10%–12% of the nickel internal demand in the US in 2030, and 15%–18%, 9%–11%, and 15%–17%, respectively, in 2035, could be met by a retired supply, assuming a closed-loop recycling system [15]. However, one of the challenges for recycling these devices, in general, is the different configurations used in the batteries, which makes it difficult to standardize recycling methods [9,14]. These factors have led to an increase in the amount of research related to the recycling of LIBs. Currently, several LIB recycling plants are under construction or in the planning phase in several countries [5].

Mechanical, hydrometallurgical, and pyrometallurgical processes, or a combination of these processes, are then usually used in the extraction of materials from spent NCM LIBs [9]. Each of these processes has advantages and disadvantages, and their application depends on several factors (economic, technical, and social, among others). Generally, mechanical processing is used as a pretreatment to separate and concentrate the metals of interest into different fractions that, posteriorly, will be recovered by other processes. Mechanical processing includes comminution and classification processes, such as shredding, milling, screening, and others [16,17]. As a result of mechanical processing, a fraction containing a mixture of materials contained in the cathode and anode and impurities is obtained; this fraction is known as black mass and can subsequently be treated hydrometallurgically to obtain the metals of interest [18].

Thus, the objectives of this study were to develop a route of mechanical pretreatment to segregate groups of materials, increase the concentration of metals into different fractions, and determine the potential of the fractions obtained through the mechanical treatment process. The prospective evaluation of particle size fractions derived from mechanical pretreatment has been devised to delineate priority fractions for recycling, incorporating considerations of (1) economic viability, (2) environmental impact, and (3) supply risk factors. The potential assessment, considering the three factors (economic, environmental, and supply), is an aspect especially important but few times explored in the literature. The main novelty of the study was the assessment to identify the particle size fractions, which are obtained by mechanical pretreatment, which are priorities for recycling for decision-making by recycling companies, optimizing their resources and efforts. Additionally, the economic, environmental, and scarcity assessment of the black mass obtained by pretreating

NCM cells was compared with the same assessment carried out on the black mass obtained by pretreating LFP cells in the previous study of Camargo et al. (2024) [19] since both cells are the most common on the market [10].

2. Material and Methods

The methodology of research and the lithium cells employed are depicted in Figure 2a.

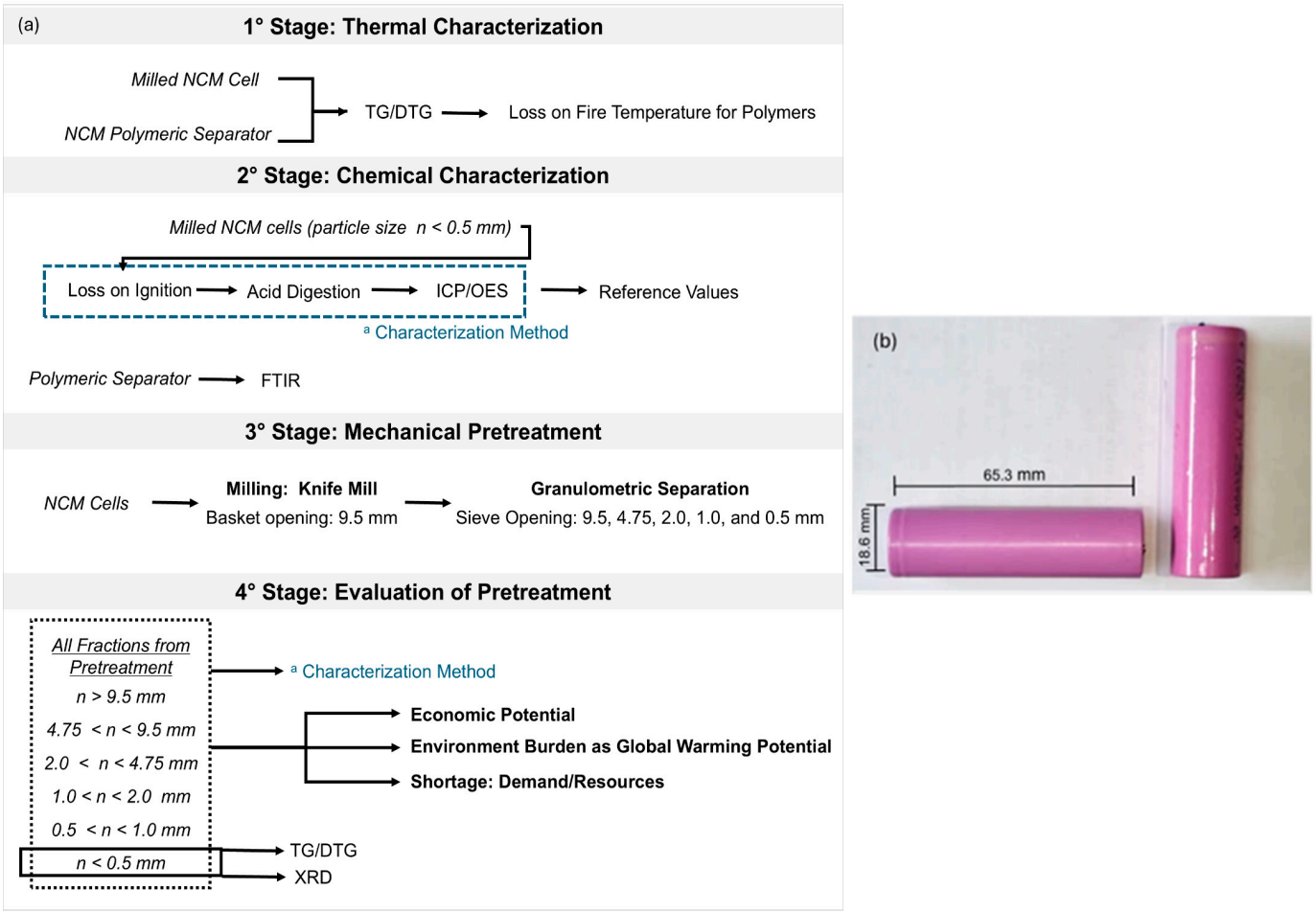

Figure 2. (**a**) Methodology, and (**b**) photography of the spent NCM cells used in this study. [a] Characterization method.

In this work, 22 spent lithium cells (around 1 kg) were employed. The cells have previously been used in micromobility equipment such as scooters and bicycles (Figure 2b). The cells are cylindrical and have nickel cobalt manganese (NCM) cathode material. The cells are 18,650-type batteries, with dimensions of 18.6 mm in diameter and 65.3 mm in length, manufactured in China in 2023, featuring a nominal capacity of 2200 mAh, 3.7 V voltage, and weighing 45 g. It is important to eliminate residual voltage from lithium cells so that they can be ground safely, avoiding explosions. In this work, the electric discharge in saline solution was not carried out to avoid contamination or loss of materials. For this reason, the cells (arranged in series) were discharged by resistors [20–22].

2.1. Characterization of NCM Cells

This preliminary study characterized the composition of Li-ion cells with nickel cobalt manganese cathode material to obtain reference values to evaluate the effectiveness of mechanical pretreatment (Figure 2a).

2.1.1. Thermogravimetric Analysis and Loss on Ignition Temperature

One of the aims of the mechanical pretreatment proposed in this work was to mill the NCM cells into a larger particle size to keep the polymeric separators in larger particle size fractions, reducing their contamination in the finer fractions. To assess the quantity of these polymers, such as polypropylene and polyethylene, loss-on-fire tests were carried out. To define the ideal loss-on-fire temperature, two TG/DTG analyses were carried out under an oxidizing atmosphere: (1) a sample of 17.8270 mg of a milled NCM cell, whose particle size was $n < 0.5$ mm, and (2) a sample of 31.4330 mg of cell separator, whose fragment was obtained by manually disassembling the cell. In these analyses, an equipment model Q50 from TA Instruments (LACOR, Porto Alegre, Brazil) was used, and the heating rate was 20 °C·min^{-1}. The TG/DTG was carried out with a synthetic air flow of 90 mL·min^{-1} in an alumina crucible with a diameter of 10 mm [23,24]. Based on the thermogravimetric analysis, a temperature was defined to carry out the loss on ignition (LoI) and identify the percentage mass for all samples in this study, aiming to establish a parameter that indicates the number of polymers. The characterization of the cell separator was carried out separately from the ground cell in order to verify the best degradation temperature for this polymeric material, aiding in the definition of the temperature used in the loss on ignition. In addition, this TG/DTG was carried out to correlate it with the mass losses that occur in the milled material.

2.1.2. Chemical Characterization of NCM Cells

A total of 11 (average mass of 45 g and a total mass of about 500 g) NCM cells were comminuted in a knife mill (Retsch model SM300, RETSCH, Haan, Germany) with a rotation speed of 1500 rpm. After quartering, 6 samples of approximately 5 g each were subjected to LoI in a muffle furnace at the temperature identified in the thermogravimetric analysis of the separators for 1 h under an oxidizing atmosphere. Afterward, the 6 samples underwent acid digestion with aqua regia for 2 h (40 mL/g sample) at the temperature of 70–80 °C. After filtration, the liquid fraction was analyzed by Inductively Coupled Plasma Optical Emission Spectrometry (ICP-OES) by the Agilent model 5110 (LACOR, Porto Alegre, Brazil). The metal concentrations measured were set as reference values to evaluate the mechanical pretreatment. The amount of graphite present in the anode material was not measured (Figure 2a).

In addition, the polymeric separator of the NCM cell, which was removed manually and characterized separately, was chemically identified using Fourier transform infrared spectroscopy (FTIR) analysis (Figure 2a). The FTIR spectrophotometer used was a Perkin Elmer Spectrum 1000 model (LACOR, Porto Alegre, Brazil), using the horizontal ATR accessory (H-ATR).

2.2. Mechanical Pretreatment for Recycling

The mechanical pretreatment involved milling 11 NCM cells for a single cycle using a Retsch model SM300 knife mill (rotation speed of 1500 rpm), whose basket opening was 9.5 mm, operating at a feed rate of 10 g·min^{-1}. After the milling was finished, the material was sieved into a series of bench sieves with a vibration system. The feed rate was 50 g/15 min, and the sieve aperture sizes were 9.5, 4.75, 2.0, 1.0, and 0.5 mm. The electromagnetic sieve shaker for particle size analysis was from the Bertel brand (Figure 2a). The mass percentage of each granulometric fraction was calculated [19].

2.2.1. Chemical Evaluation of All Fractions

Following homogenization, quartering, and comminution of the granulometric fractions from mechanical pretreatment, 3 samples of 5 g from each fraction underwent LoI, acid digestion, and analysis by ICP-OES (LACOR, Porto Alegre, Brazil), following the same procedures as previously reported (Figure 2a). The concentrations (% by mass) of each fraction of LoI, aluminum, cobalt, copper, iron, lithium, manganese, and nickel were calculated.

A fraction may have a high concentration of the material of interest but have a relatively low mass in relation to the total amount of cells processed. For this reason, calculating the mass percentage distribution of the element (metals and LoI) is important to check whether the mechanical pretreatment has been effective in separating and concentrating it. The mass percentage distribution of each element within each fraction was calculated using Equation (1):

$$D^e_{fn}(\%) = 100 \times \frac{C^e_{fn}(\%) \times P_{fn}(\%)}{\sum_{n=1}^{6} C^e_{fn}(\%) \times P_{fn}(\%)}, \quad (1)$$

where

D^e_{fn} : Mass percentage distribution of element "e" in fraction "n", in %;

C^e_{fn} : Average percentage concentration of element "e" in fraction "n", identified by ICP-OES;

P_{fn} : Mass percentage of the "n" particle size fraction in relation to the quantity of cells processed in mechanical pretreatment;

$\sum_{n=1}^{6} C^e_{fn} \times P_{fn}$: Sum of all six concentration products of the element "e" in each fraction by the percentage of each fraction.

To assess the potential of the pretreatment developed, the mass (in kg) of each element of interest (metals and LoI) contained in each of the different particle size fractions was estimated if 1000 kg of the NCM cells studied were processed, using Equation (2).

$$M^e_{fn}(\text{kg}) = 1000(\text{kg}) \times [\frac{C^e_{fn}(\%)}{100}] \times [\frac{P_{fn}(\%)}{100}]$$

or

$$M^e_{fn}(\text{kg}) = [\frac{C^e_{fn}(\%) \times P_{fn}(\%)}{10}], \quad (2)$$

where

M^e_{fn} : Mass of element "e" in fraction "n" if 1000 kg of the NCM cells studied were processed in kg;

C^e_{fn} : Average percentage concentration of element "e" in fraction "n", identified by ICP-OES, in %;

P_{fn} : Mass percentage of the "n" particle size fraction in relation to the number of cells processed in mechanical pretreatment, in %.

2.2.2. Black Mass (Fraction n < 0.5 mm): TG/DTG and X-Ray Diffraction

The black mass from mechanical pretreatment underwent a TG/DTG analysis (Figure 2a) using the Q50 model from TA Instruments (LACOR, Porto Alegre, Brazil), whose temperatures varied from 0 to 900 °C under a heating rate of 20 °C·min^{-1} The mass of the sample was 14.4070 mg, and the TG/DTG was carried out with a synthetic air flow of 90 mL·min^{-1} in an alumina crucible with a diameter of 10 mm.

For the X-ray diffraction analysis (XRD) (Figure 2a), the black mass sample was macerated in an agate mortar to achieve a particle size of 0.045 mm (325 mesh). The analysis was performed by the Panalytical equipment, Aeris model, using a Cu source (with Cu-Kα radiation source with λ = 1.54 Å), with the detector refined to the PHD range 8–11.27 kV, a step size of 0.022°, and a 2θ angular interval from 15° to 85°.

2.2.3. Economic, Environmental, and Shortage Potential Evaluation

These assessments were carried out using the methodology developed by Cenci et al. (2024) [25].

Economic Potential

The economic potential parameter relates to the market worth of materials based on their quantities within the fractions of the most efficient recycling processes. The economic value (EV) of each material (m) is derived by multiplying the mass fraction of that material

by its market price (Table 1), as expressed in Equation (3). The values were normalized to the base of 1000 kg.

$$EV^{e}_{fm}(\text{USD}) = M^{e}_{fn}(\text{kg}) \times CF^{m}_{e} \times MV_{m}\left(\frac{\text{USD}}{\text{kg}}\right), \quad (3)$$

where

EV^{e}_{fn} : Economic value of each material in fraction "n" if 1000 kg of the NCM cells studied were processed;

M^{e}_{fn} : Mass of element "e" in fraction "n" if 1000 kg of the NCM cells studied were processed;

CF^{m}_{e}: Mass conversion factor from element "e" to material "m";

MV_{m}: Market value of material "m"

Table 1. Materials analyzed with their mass conversion factors and market values in USD/kg.

Element	Material	Mass Conversion Factor	Market Value (USD/kg)
Al	Aluminum	1	2.290 [1]
Co	Cobalt	1	26.625 [1]
Cu	Copper	1	9.10 [1]
Fe	Steel Rebar	1	0.425 [1]
Li	Li_2CO_3	5.322	11.78 [1]
Mn	Mn_2O_3	4.260	1.25 [2]
Ni	Nickel	1	15.80 [1]

Sources: [1] (Daily Metal Prices, 2024) [26]; [2] (Business Analytiq, 2024) [27].

For all materials except manganese, the market values were sourced from the Daily Metal Prices website [26], whose values were collected in July 2024. For the element Li, the values were obtained from compounds Li_2CO_3 and required a mass conversion to an elementary base. For manganese, the market value was sourced from the Business Analytiq website [27], whose value was found in July 2024. The value was obtained from compound Mn_2O_3 and required mass conversion to an elementary base. All other elements assumed 99% purity. This assessment of economic potential does not factor in the expenses associated with recovery processes and the manufacturing of raw materials derived from mechanically pretreated materials. Additionally, this calculation does not account for material losses. The aim of the economic potential estimative was to identify the priority fractions obtained through pretreatment for recycling based on economic considerations.

Environmental Burden as Global Warming Potential

Each material carries an environmental burden (EB_m) through its life cycle.

Equation (4) assesses the environmental burden in the cradle-to-gate approach by multiplying the environmental impact (*GWP* in this study) by the mass fraction.

$$EB(GWP)_{m} = GWP_{m}\left(\frac{\text{kg}CO_2\text{eq}}{\text{kg}}\right) \times M^{e}_{fn}(\text{kg}), \quad (4)$$

where

$EB(GWP)_{m}$: Environmental burden of material "m"

GWP_{m}: Global warming potential of material "m"

M^{e}_{fn}: Mass of element "e" in fraction "n" if 1000 kg of the NCM cells studied were processed;

Global warming potential (GWP) values were collected from the study of Nuss and Eckelman (2014) [28]. This approach highlights materials with a high environmental burden associated with primary ore treatment, making them attractive for recycling. Other environmental impact categories could be considered, such as land use, acidification, and ecotoxicity. The calculation used the following values in kg CO_2-eq/kg: 8.8 for Al, 8.3 for Co, 2.8 for Cu, 1.5 for Fe, 7.1 for Li, 1.0 for Mn, and 6.5 for Ni. The values were adjusted in

relation to the mass percentage of each fraction to inform the kilograms of CO_2-eq per ton of NCM cells processed. The objective of the environmental burden as a global warming potential estimate was to identify the priority fractions obtained through pretreatment for recycling based on environmental considerations.

Shortage

Equation (5) evaluates material scarcity by integrating factors associated with raw material shortages, market shortages connected to supply risks, and the significance of scrap. The variables α, β, and γ denote the weights assigned to each criterion. In this study, weights of 1 were assigned to α and γ, while β received a weight of 3 to highlight the importance of supply risk. Alternative weight values may be employed as needed.

$$\mathrm{SR}_m = 10^4 \times \left(\frac{Demand_m(\mathrm{ktons})}{MineralResources_m(\mathrm{ktons})} \right)^{\alpha} \times (SupplyRisk_m)^{\beta} \times \left(\frac{MassFraction_m(\%)}{Demand_m(\mathrm{ktons})} \right)^{\gamma}, \quad (5)$$

where

SR_m^e: Shortage Risk Index

The equation assesses the portion of accessible mineral resources needed for upcoming applications, integrating data from research on future demand covering the years 2016 to 2050 [29,30]. Due to geopolitical differences, the supply risk values specific to the European Union were considered. In this context, the mass fraction relative to demand focuses on materials that have a significant potential for recovery from scrap. Adjustments were made to the values based on the mass percentage of each fraction, which helps identify the priority fractions for recycling derived from mechanical pretreatment while considering the associated supply risks.

3. Results and Discussion

3.1. Characterization of NCM Cells

3.1.1. Thermogravimetric Analysis and Loss on Ignition Temperature

By the TG/DTG analysis of the milled cell (Figure 3a), the beginning of the thermal decomposition process was observed with a slight weight loss below 200 °C, which can be attributed to residual electrolyte [31]. A second weight loss, more pronounced (approximately 8.0%), was observed between 225 and 600 °C (Figure 3a,b) and was attributed to the decomposition of polymeric materials such as polyethylene (PE) and polyvinylidene fluoride (PVDF) [32,33]. The third weight loss (approximately 13.5%) was observed between 600 and 800 °C and can be attributed to the oxidation of graphite [34,35]. Also, a high percentage (approximately 75%) of residual material was observed at 800 °C. This high percentage of undecomposed material can be attributed to the inorganic fraction or metallic material in the sample. A slight increase in mass was identified above 800 °C, with a value of 75% at 800 °C rising to 76.3% at 900 °C. This increase in mass was due to the oxidation of the metals present. In this temperature range from 800 °C to 900 °C, there was competition for the available oxygen. On the one hand, the carbon in the graphite was turning into CO or CO_2, and on the other, the metals were oxidizing [36].

In the TG/DTG analysis of the cell polymeric separator (Figure 3b), there was also a first stage below 225 °C and a second stage, 225–600 °C, similar to the stages seen in the TG analysis of the milled cell (Figure 3a). In the second stage, the weight loss was more evident (approximately 45.0%) and can be attributed to the decomposition of polymeric material from the separator. In the DTG analysis, it is possible to observe two peaks in the second stage, which indicates that the separator is made of polyethylene and polyvinylidene fluoride (PE/PVDF) [32]. Furthermore, it is possible to observe a high residue (approximately 47.0%) that can be attributed to the presence of inorganic material in the separator. Nanoparticles of aluminum oxide (Al_2O_3) or silicon oxide (SiO_2), for example, are used in some types of separators to improve some of their properties [37,38].

The aim of the LoI temperature was to quantify the polymers in the separator in particular. In the TG/DTG of the polymeric separator (Figure 3b), the temperature of

600 °C was the one identified to obtain the maximum degradation of these polymers. The temperature of 800 °C, which was identified in the TG/DTG of the milled cell (Figure 3a), was not used like the LoI temperature. By analyzing these results (Figure 3b), it was possible to establish that 600 °C was the ignition loss temperature to be used in the samples throughout the study.

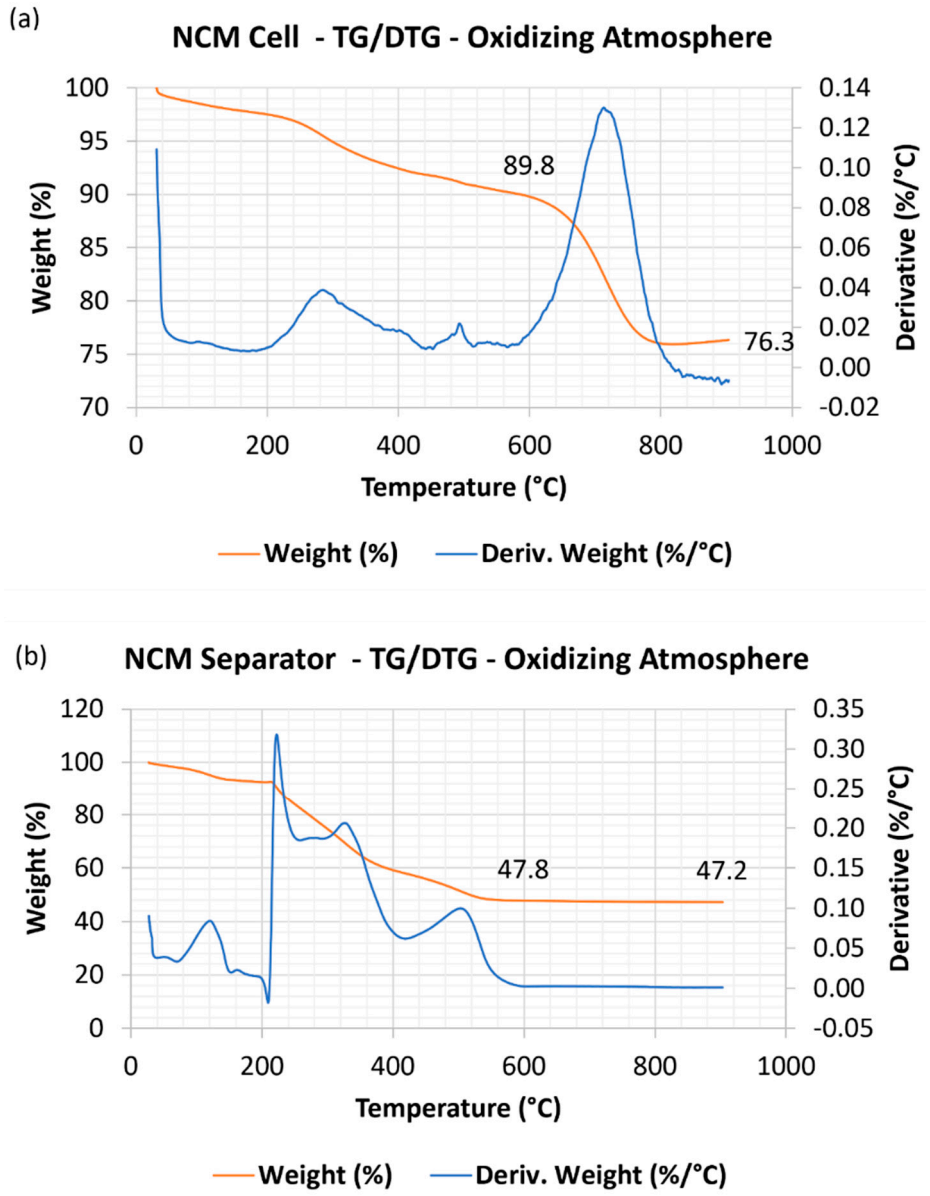

Figure 3. TG/DTG analysis under an oxidizing atmosphere of (**a**) milled NCM cell, whose particle size was $n < 0.5$ mm (**b**) cell separator, whose fragment was obtained by disassembling the cell.

3.1.2. Chemical Characterization of NCM Cells

Figure 4a shows the mass percentage and their standard deviations of LoI, aluminum, cobalt, copper, iron, lithium, manganese, and nickel in the NCM cells studied. The percentage leached from the samples of milled NCM cells subjected to acid digestion was 93.7 ± 0.9%. In Figure 4a, the percentage of LoI corresponds to the thermally degraded material in the TGA of Figure 3a. Given the contribution of the LoI in the cell mass, an FTIR analysis was performed, aiming to discover its composition.

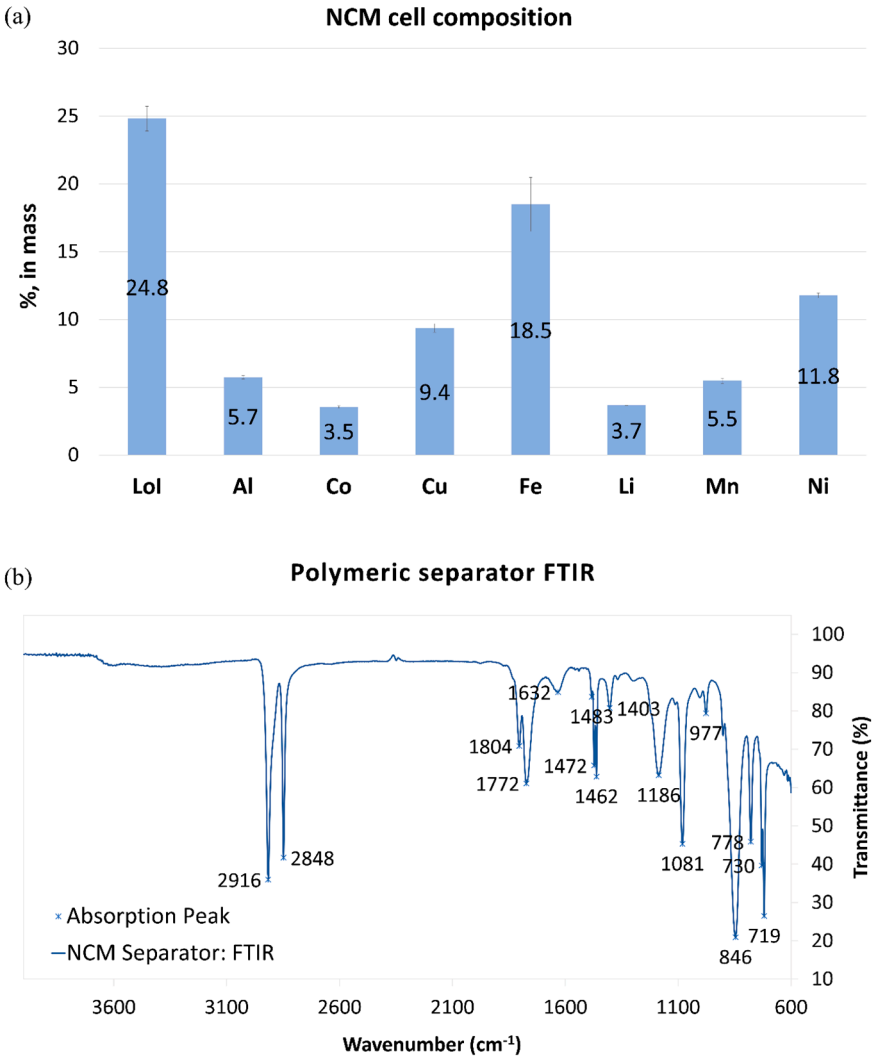

Figure 4. (**a**) Mass percentage and their standard deviations of LoI at 600 °C, aluminum, cobalt, copper, iron, lithium, manganese, and nickel in the NCM cells studied. LoI indicates the polymers of separators, binders, and organic electrolytes thermally degraded at 600 °C. (**b**) FTIR analysis of the separator of the NCM cell studied.

Figure 4b shows the FTIR of the separator from the NMC cell studied. The absorption bands in 2916 and 2848 cm^{-1} can be attributed to CH_2 asymmetric and symmetric stretching, bands in 1462 and 1472 cm^{-1} to the bending deformation CH_2, and bands in 730 and 719 cm^{-1} to the rocking deformation; all these bands are typical of polyethylene (PE) [39–42]. However, absorption bands in 1403 cm^{-1} can be attributed to the bending deformation of CH_2, 1186, and 1081 cm^{-1} to the symmetric stretching vibration of CF_2. Furthermore, the bands in 778, 846, and 977 cm^{-1} are typical of polyvinylidene fluoride (PVDF) [43–45]. Thus, it is possible to state that the separator is composed of PE coated with PVDF. The other absorption bands can be attributed to the presence of residual carbon and Al_2O_3, corroborating the results observed in the TGA analysis of the separator (Figure 4b).

3.2. Mechanical Pretreatment for Recycling

3.2.1. Chemical Evaluation of All Fractions

The fractions obtained by pretreatment can be seen in Figure 5a.

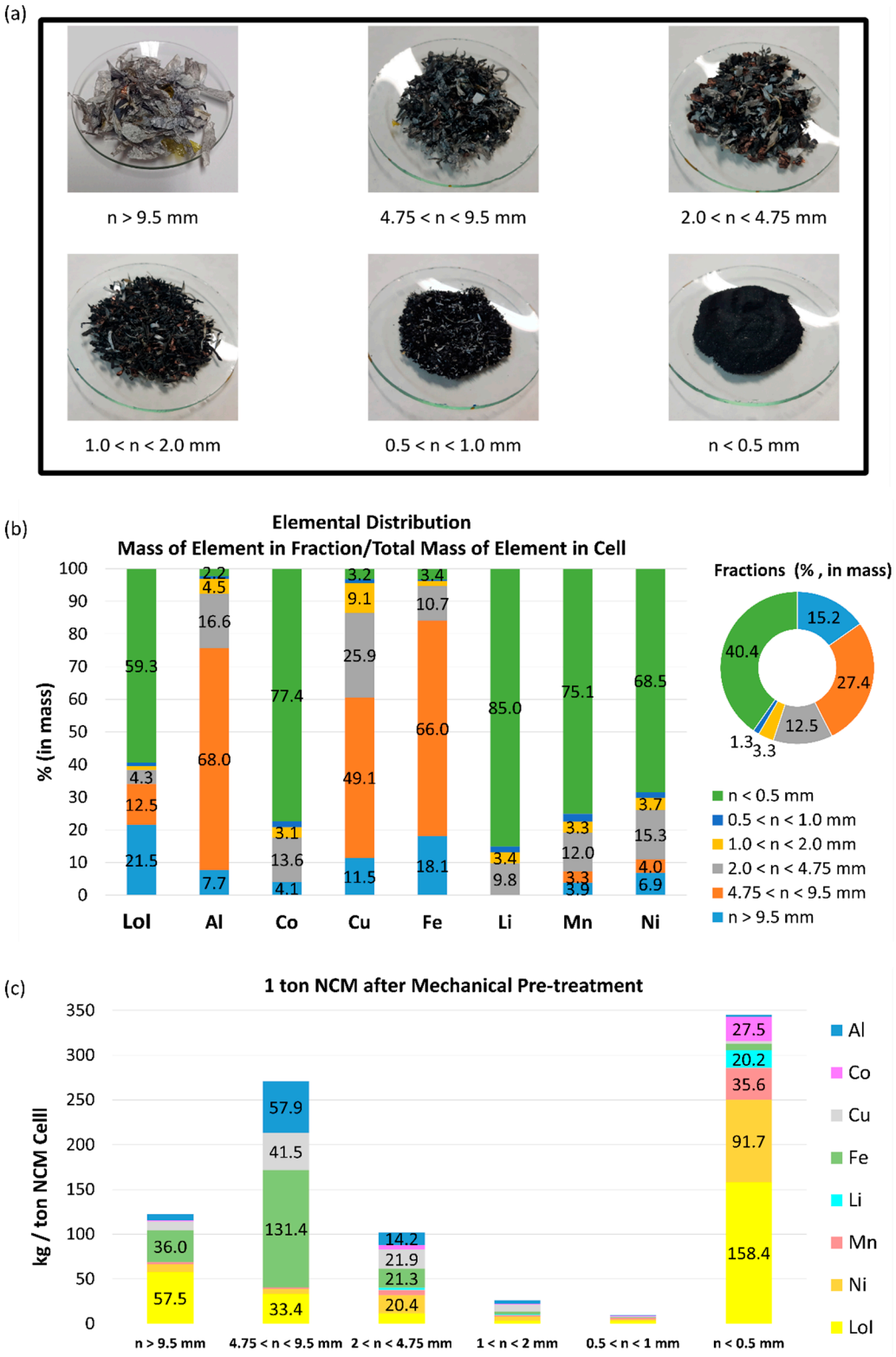

Figure 5. (**a**) Particle size fractions obtained by mechanical pretreatment of grinding and sieving of NCM cells. (**b**) Percentage mass distribution of the main elements in the granulometric fractions obtained by mechanical pretreatment. The data show the ratio of the mass of the element found in the fraction to the total mass of the element identified in the characterization of the NCM cell. (**c**) Distribution in kilograms of metals and LoI in each particle size fraction for 1 ton of processed NCM cells. LoI indicates the polymers of separators, binders, and organic electrolytes thermally degraded at 600 °C.

In the $n > 9.5$ mm fraction, there was a notable amount of polymer bands (white color) coming from the separators. It was observed that the white material (polymeric separators) content decreased as the particle size decreased, indicating a tendency for these polymers to concentrate in the coarser fractions. The ductility of polymeric separators, an inherent property of thermoplastic materials, results in low brittleness, leading to a reduced grinding efficiency and particle size reduction during the knife mill process. The LoI parameter was an indication of the mass percentage of this separator.

The amount of electrolytes and binders has not been measured or determined. However, the literature reports that these compounds are originally associated with the active materials of the cathode and anode [2]. Consequently, the electrolyte and binder are expected to be together in the black mass. The $n < 0.5$ mm fraction was rich in cathodic and anodic material, and consequently, the binder and residual organic electrolyte were present in them (Figure 5a).

The concentrations of each fraction are presented in Table 2.

Table 2. Percentage concentration (by mass) of the particle size fractions obtained by pretreatment in the NCM cells studied.

	Concentrations of the Fractions Obtained by Mechanical Pretreatment (%, in Mass)					
	$n > 9.5$ mm	**$4.75 < n < 9.5$ mm**	**$2 < n < 4.75$ mm**	**$1 < n < 2$ mm**	**$0.5 < n < 1$ mm**	**$n < 0.5$ mm**
LoI	37.8 ± 5.6	12.2 ±0.6	9.2 ± 0.8	9.8 ± 1.6	22.3 ± 1.6	39.2 ± 1.8
Al	4.3 ± 1.3	21.1 ± 1.4	11.3 ± 1.4	11.7 ± 1.4	6.1 ± 0.9	0.5 ± 0.0
Co	1.0 ± 0.3	0.0 ± 1.3	3.9 ± 0.6	3.3 ± 0.5	5.0 ± 0.8	6.8 ± 1.6
Cu	6.4 ± 1.1	15.2 ± 10.6	17.5 ± 2.3	23.4 ± 2.4	7.7 ± 1.8	0.7 ± 0.2
Fe	23.7 ± 1.7	47.9 ± 5.4	17.1 ± 2.6	9.1 ± 0.8	4.8 ± 0.3	1.7 ± 0.9
Li	<LD	<LD	1.9 ±0.3	2.4 ± 1.0	3.4 ± 0.6	5.0 ± 1.1
Mn	1.2 ± 0.3	0.6 ± 0.2	4.6 ± 0.3	4.8 ± 0.3	8.7 ± 1.4	8.8 ± 1.8
Ni	6.1 ± 1.2	2.0 ± 0.2	16.4 ± 1.2	15.1 ± 1.5	16.7 ± 1.7	22.7 ± 1.1

The percentage leached from the samples subjected to acid digestion was 98.5 ± 1.5% for $n > 9.5$ mm, 97.4 ± 2.1% for $4.75 < n < 9.5$ mm, 95.2 ± 1.2% for $2 < n < 4.5$ mm, 92.5 ± 1.4% for $1 < n < 2$ mm, and 98.0 ± 0.3 for $n < 0.5$ mm.

The fraction $n < 0.5$ mm had 39.2 ± 1.8 of LoI, which was associated with the amount of binder, graphite, and some residual electrolyte. On the other hand, the fraction $n > 9.5$ mm had 37.8 ± 5.6 LoI, which was associated with the polymeric separator (Table 2 and Figure 5a). The fraction $1 < n < 9.5$ mm had the highest concentration of aluminum and copper. And the $n > 4.75$ mm fraction had the highest concentration of iron.

The $n < 0.5$ mm fraction, the black mass, had 22.7% nickel, 8.8% manganese, 6.8% cobalt, 5.0% lithium, 0.7% copper, 0.5% aluminum, and 39.2% LoI. Dadé et al. (2022) analyzed via ICP-OES the composition of black mass produced by treatments such as pyrolysis, dry shredding, and sieving and identified 21.40% nickel, 7.50% manganese, 7.27% cobalt, 9.78% lithium, 1.98% copper, 7.98% aluminum, and 40.80% carbon. The results were similar, but the $n < 0.5$ mm fraction had a lower concentration of lithium, and it was less contaminated with aluminum and copper [46].

In the study of Mousa et al. (2023), two grades of battery materials (BM1 and BM2) were collected from a recycling facility that processes spent Li-ion batteries (LIBs) through dry mechanical methods, including crushing, sieving, and magnetic separation. BM1 and BM2 represented the undersized fractions (<4.0 mm) from sieving, concentrating cathode materials (LiM_eO_x), and anode materials (graphite). The ICP-OES analysis indicated that BM1 had a chemical composition of 5.1% nickel, 3.0% manganese, 17.5% cobalt, and 3.9% lithium, among other components. The chemical analysis of BM2 revealed 12.5% nickel, 10.9% manganese, 5.4% cobalt, and 2.6% lithium, among other constituents. The findings indicated a higher cobalt content, while BM2 contained higher levels of nickel and manganese, suggesting different NMC battery types [47].

During milling, the electrolyte did not react or damage the stainless steel mill. Most of the electrolyte was evaporated and was captured by the exhaust system. On a laboratory scale, the quantification and environmental and economic evaluation of the electrolyte was not contemplated because of its high volatility and consequent rapid evaporation during the milling process. The residual electrolyte that remained in the fractions was not in liquid form, and the fractions obtained by pretreatment were dry and unchanged. On a laboratory scale, a gas scrubber was not necessary, but a gas scrubber is essential on an industrial scale. The aim of this study was not to propose the recovery of the electrolyte, but the collection and condensation of these vapors during milling on an industrial scale is important for its recovery. Many industrial shredding centers are beginning to make use of emission controls such as enhanced air handling and suction systems like cyclones, scrubbers, and baghouse filters [48]. Elemental distribution in each particle size fraction obtained by mechanical pretreatment is shown in Figure 5b. The value reported indicates the percentage in relation to the total amount of the element present in the entire cell that was concentrated in each particle size fraction. These results are fundamental to verifying the separation efficiency of mechanical pretreatment. The fraction $1 < n < 9.5$ mm had 89% of the total amount of aluminum in the cell, and 11% was lost to other fractions. A total of 84% of all copper was also separated in $1 < n < 9.5$ mm, and 16% was lost to other fractions. In addition, 95% of all iron remained in the $n > 2$ mm fraction, and 5% was lost to other fractions (Figure 5b). The mechanical process adopted, based on grinding and sieving, showed 3.9% losses in the form of dust to the environment. In various comminution processes, material losses can primarily happen during the grinding phase. Fine particles may escape from the mills and become drawn into the exhaust system. Hence, mills must be designed to minimize environmental losses. Some cathode-active material might be lost to the coarser fractions. However, this material generally tends to accumulate in finer fractions. As can be seen in Figure 5b, 85% of all lithium in the cell was concentrated in the fraction with a particle size $n < 0.5$ mm, and the remaining 15% of lithium was lost in fractions $n > 0.5$ mm. Moreover, 77.4% of cobalt, 75.1% of manganese, and 68.5% of the nickel of the entire cell were concentrated in the $n < 0.5$ mm fraction. This fraction showed low contamination values for aluminum (2.2%), copper (3.2%), and iron (3.4%), whose percentages are related to the total element content of the entire cell. The fraction $n < 0.5$, which can be called the black mass, represented 40.4% of the mass of all the cells processed.

This study focused on mechanically processing cylindrical cells, but pouch and prismatic cells have different casing materials that affect the composition of the coarser fraction, where materials like steel, aluminum, and polymers are concentrated. Recycling processes may vary with these cell types due to differences in the casing size and composition, leading to differences in particle size distribution across product fractions. Prismatic cells with a steel casing require more energy than prismatic cells with an aluminum casing. Cylindrical cells require a similar crushing energy than prismatic cells, and pouch cells have a comparably low energy consumption. The particle size distribution varies quite significantly between the different cell types, which is mostly caused by the amount of material $n < 1$ mm being created. This is caused by significant differences in the decoating for the different cell types, especially of the cathodes [20,49–52]

The estimated amount of material separated into each fraction if 1000 kg of milled NCM cells were subjected to the same process is reported in Figure 5c. The figures do not consider losses since this factor depends on operating conditions. For each ton of pretreated cell, 188.7 kg of iron, 102.4 kg of polymers, 78.6 kg of aluminum, and 73.1 kg of copper would be generated at $n > 2$ mm. For each ton of cell processed, the black mass ($n < 0.5$ mm) would contain 27.5 kg of cobalt, 20.2 kg of lithium, 35.6 kg of manganese, and 91.7 kg of nickel, for a total of 174.9 kg of cathode material. This cathode material would be contaminated with 2.0 kg of aluminum, 2.8 kg of copper, and 6.9 kg of iron (Figure 5c). It would not be possible to recover 100% of these metals in subsequent recovery processes (via hydrometallurgy and pyrometallurgy, for example) as there are always losses. However, this study serves as an indication of the granulometric fraction richest in certain metals.

3.2.2. Black Mass (Fraction $n < 0.5$ mm): TG/DTG and X-Ray Diffraction

The DTG in Figure 6a shows a large peak observed at 710 °C that can be attributed to the LoI maximum decomposition rate. The 37.5% mass loss of this peak is compatible with the LoI percentage of 39.2 ± 1.8% (Table 2).

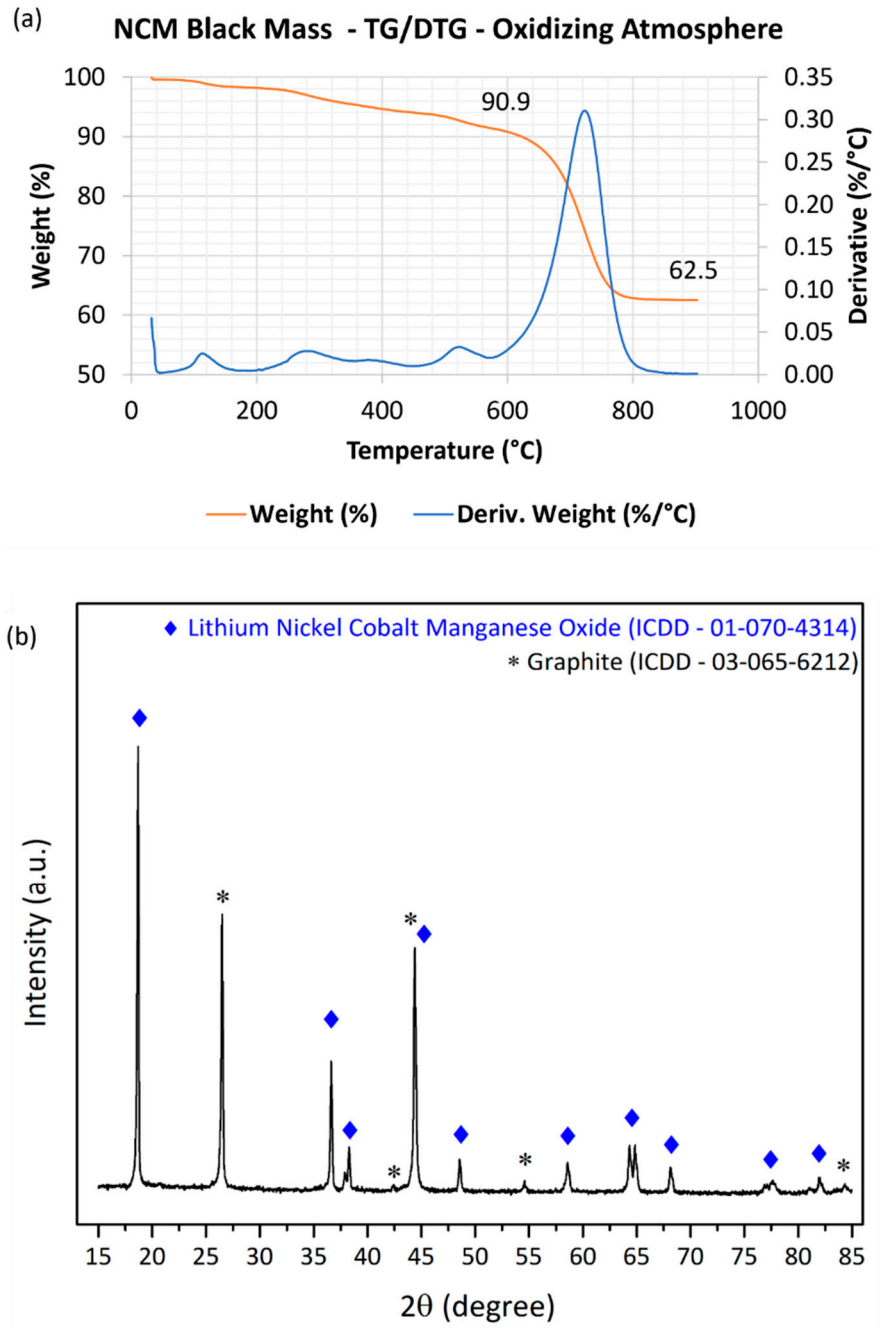

Figure 6. (**a**) TG/DTG analysis of black mass, under an oxidizing atmosphere, which was obtained by mechanical pretreatment ($n < 0.5$ mm). (**b**) X-ray diffraction (XRD) analysis of the black mass obtained by mechanical pretreatment of NCM cells.

The X-ray diffraction (XRD) analysis of the black mass obtained by mechanical pretreatment revealed the presence of two crystalline phases. Graphite was identified, characterized by the crystallographic pattern ICDD 03-065-6512, and lithium–nickel–cobalt–manganese oxide, identified by the crystallographic pattern ICDD 01-070-4314, with a chemical composition of $Co_{0.1}Li_{1.03}Mn_{0.1}Ni_{0.77}O_2$, characteristic of the NMC_{811} cathode material type (Figure 6b).

3.2.3. Economic, Environmental, and Shortage Potential Evaluation

The potential evaluation of the particle size fractions obtained by mechanical pretreatment (Figure 7) was designed to indicate the priority fractions for recycling, considering economic (Figure 7a), environmental (Figure 7b), and supply risk aspects (Figure 7c). The values given indicate the order of magnitude since they do not consider (1) process losses, (2) the efficiency of recovery of the metals mentioned, (3) economic costs, and (4) greenhouse gas emissions from subsequent recycling stages. This analysis did not account for polymers, graphite, or electrolytic solutions.

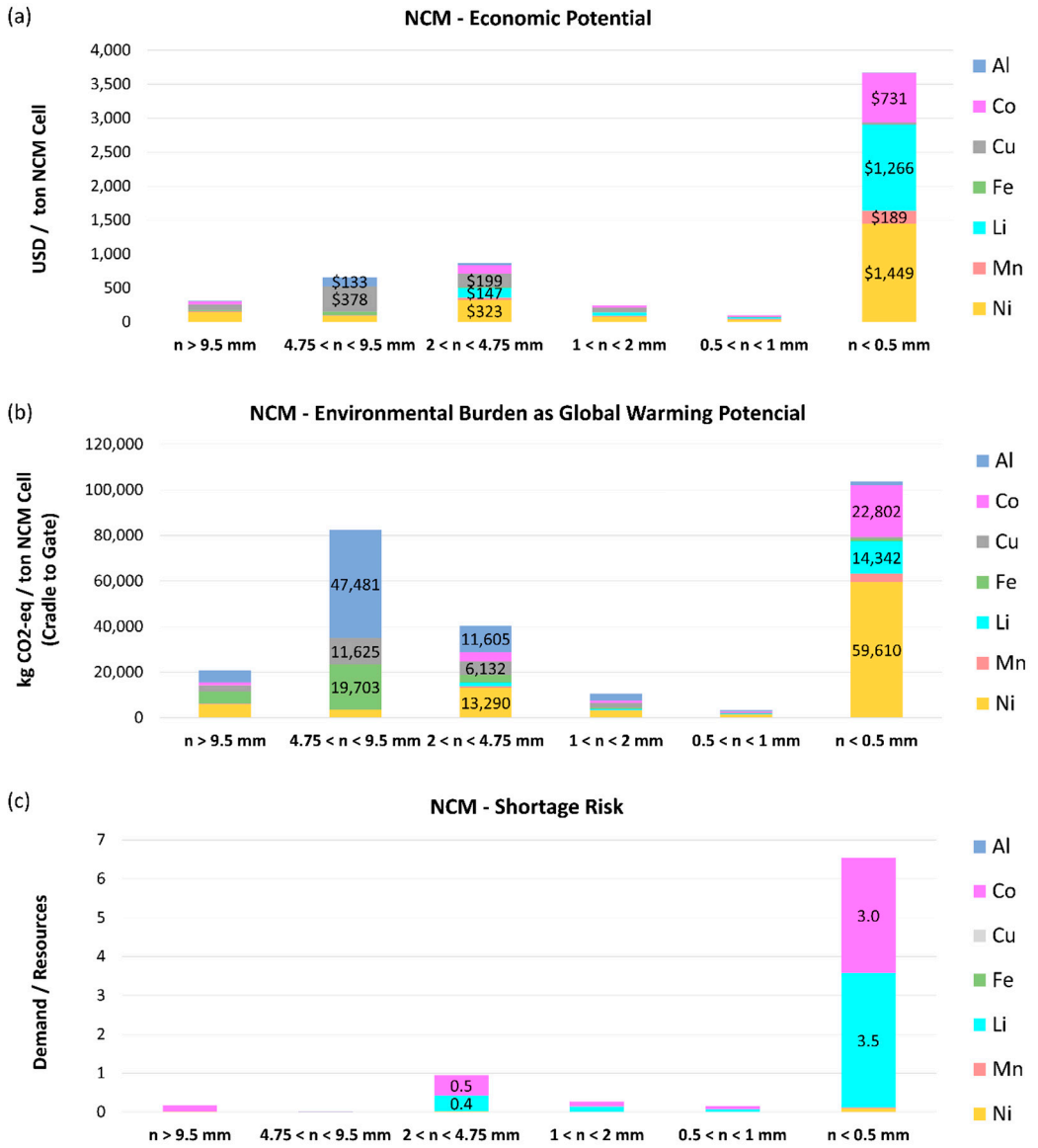

Figure 7. (**a**) Economic potential (in US dollars) of the particle size fractions obtained by processing 1 ton of NCM cells. (**b**) Environmental burden as global warming potential (in kg CO_2-eq/ton NCM Cell) of the particle size fractions obtained by processing 1 ton of NCM cells. (**c**) Shortage risk index according to the fractions obtained by mechanical pretreatment.

Economic Potential

As can be seen in Figure 7a, fraction $n < 0.5$ mm had the highest economic potential (USD 3669/ton NCM cell), which was four times more than the second-highest potential fraction, which was $2 < n < 4.75$ mm (USD 870/ton NCM cell). Table 2 shows that there were around 16.4 ± 1.2% of nickel in the fraction $2 < n < 4.75$ mm. Consequently, in Figure 7a,

this fraction has the second highest economic potential, mainly because of the nickel (USD 323/ton NCM cell). Although the fractions $1 < n < 2$ mm and $0.5 < n < 1$ mm have similar percentages of nickel (Table 2), these fractions are not very representative in terms of mass (Figure 5b). Consequently, they do not stand out in the analysis of economic potential (Figure 7a). Moreover, copper (USD 378/ton NCM cell) was the metal with the highest economic potential in the fraction $4.75 < n < 9.5$ mm (Figure 7a).

The fraction of black mass ($n < 0.5$ mm) obtained by the same mechanical process but from LFP cells ranged from 881 to 1120 USD/ton LFP cell [19]. This elevated economic potential of the black mass from NCM cells was due to the market value of cobalt (26.62 USD/kg) and lithium carbonate (11.78 USD/kg), both of which are critical raw materials, in addition to nickel (15.80 USD/kg). These results show that the black mass of NCM cells has greater economic potential than the black mass of LFP cells, not considering the costs of the recycling process. Consequently, more complex recycling processes can be used on NCM cells than on LFP cells, and LFP cells need to be treated by processes with lower economic costs to make recycling economically viable because they result in lower value-added products.

The greatest economic potential lies in the black mass from $n < 0.5$ mm (USD 3669/ton NCM cell), but an important part lies in the other fractions, especially $2 < n < 9.5$, which accounted for 39.9% of the cell mass (Figure 5b). The fraction $2 < n < 9.5$ had an estimated economic potential of USD 1529/ton NCM cell or 41.7% of the economic potential of fraction $n < 0.5$ mm. This study indicates that black mass ($n < 0.5$ mm) is the priority fraction, but the forwarding of other fractions for specific recycling processes is perfectly feasible through mechanical pretreatment. Wang et al. (2016) also proposed a pretreatment of mechanical shredding and sorting steps based on size and explained that, instead of processing the entire spent LIBs using a single technology, several recycling processes could be integrated to target specific materials enriched in each particle size fraction (e.g., copper from the medium fractions and iron from the coarse fractions) [48].

Environmental Burden as Global Warming Potential

In the environmental assessment (Figure 7b), it was determined which fractions should be prioritized for recycling to reduce CO_2 equivalent emissions per 1 ton of NCM cells obtained through primary production. The fraction $n < 0.5$ mm represented 103,788 kg CO_2-eq/ton NCM cell, primarily due to the presence of nickel, cobalt, and lithium. In contrast, the fraction of black mass ($n < 0.5$ mm) obtained by the same mechanical process but from LFP cells ranged from 183 to 388 kg CO_2-eq/ton LFP cell [19]. These results indicate that the production of cathode material from NCM cells through primary production results in more carbon emissions than the production of cathode material from LFP cells, disregarding emissions related to the recycling process. Jiang et al. (2022) also reported that the production of LFP cells has a lower environmental impact per kilogram compared to NCM cells [13]. The recovery of valuable materials from NCM black mass has a significant multiplier effect on reducing total CO_2 emissions. NCM recycling should, therefore, be prioritized as a strategy for minimizing global environmental impact while maximizing the economic value of critical metal recovery.

The fraction $2 < n < 9.5$ mm had an environmental burden as a global warming potential of 122,925 kg CO_2-eq, primarily due to the presence of aluminum, iron, copper, and nickel (Figure 7b). The recycling of fractions $2 < n < 9.5$ mm, despite having a lower economic value, still plays a key role in reducing the CO_2 emissions associated with primary production. These fractions contain materials such as aluminum, iron, and copper, which, although not as critical as cobalt or lithium, are also valuable and can be recycled to reduce the need for mining and the corresponding environmental impacts. Adopting recycling processes that integrate these medium and coarse fractions can, therefore, help balance the economic cost with a reduction in carbon emissions.

Shortage

Among all the metals present in NCM lithium-ion cells, cobalt and lithium stand out the most in terms of supply risk. The supply risk for $n < 0.5$ mm was 6.54 (Figure 7c), seven times higher than the second-highest index fraction ($2 < n < 4.75$ mm). Moreover, the fraction of black mass ($n < 0.5$ mm) obtained by the same mechanical process but from LFP cells ranged from 1.80 to 1.84 [19]. The recovery of cobalt from NCM cells is essential to guarantee the supply of this critical raw material, as well as lithium. Therefore, the $n < 0.5$ mm fractions are the priority for recycling, considering their shortage (Figure 7c).

The elevated shortage risk index of cobalt and lithium, especially concentrated in the $n < 0.5$ mm fraction, not only highlights the importance of recovering these critical metals but also underlines the environmental benefit of recycling. By recovering these metals through recycling, rather than relying on mining, the supply chain becomes more resilient and sustainable, reducing the pressure on natural sources and the emissions associated with the primary production of these materials. Recycling these fractions is, therefore, a dual strategy: mitigating supply risks and contributing to the reduction in carbon emissions.

4. Conclusions

The mechanical pretreatment (using grinding, with a knife mill, and particle size separation by sieving) concentrated lithium nickel cobalt manganese oxide and graphite in the finest fraction (particle size $n < 0.5$ mm), which represented 40.4%, on average, of the entire mass of NCM cells processed. The fraction $n < 0.5$ mm had the highest economic potential (USD 3,669/ton NCM cell), which was four times more than the second-highest potential fraction, i.e., $2 < n < 4.75$ mm (USD 870/ton NCM cell). In the environmental assessment, fraction $n < 0.5$ mm represented 103,788 kg CO_2-eq, primarily due to the presence of nickel, cobalt, and lithium. The fraction $2 < n < 9.5$ mm had an environmental burden as a global warming potential of 122,925 kg CO_2-eq because of the presence of aluminum, iron, copper, and nickel. Among all the metals present in NCM lithium-ion cells, cobalt and lithium stand out the most in terms of supply risk. The supply risk for $n < 0.5$ mm was 6.54, seven times higher than the second-highest index fraction ($2 < n < 4.75$ mm). Moreover, the $n < 0.5$ mm fraction (black mass) was the priority for recycling and had greater economic, environmental, and supply risk potential than the black mass of LFP cells.

These findings underscore the critical importance of recycling the $n < 0.5$ mm fraction to address both economic and environmental concerns. The efficient recovery of cobalt and lithium from this fraction can significantly mitigate supply chain risks and lower CO_2 emissions associated with the traditional mining process. Additionally, the higher economic potential and environmental burden of the $n < 0.5$ mm fraction make it a prime target for technological innovations in recycling, which could improve both the profitability and sustainability of the recycling process. Recycling the $2 < n < 9.5$ mm fractions, though economically less valuable, is crucial for reducing CO_2 emissions by recovering materials like aluminum, iron, copper, and nickel, thus minimizing the need for mining and its environmental impact.

Author Contributions: Conceptualization: P.S.S.C. and H.M.V.; Methodology: P.S.S.C. and M.P.C.; Formal analysis and investigation: P.S.S.C., M.H.C., R.d.R.C., A.C.K., and F.A.L.S.; Writing—original draft preparation: P.S.S.C., M.H.C., R.d.R.C., and A.C.K.; Writing—review, and editing: P.S.S.C., A.C.K., F.A.L.S., and H.M.V.; Funding acquisition: H.M.V.; Resources: H.M.V.; Supervision: H.M.V. All authors have read and agreed to the published version of the manuscript.

Funding: The work was funded by the Brazilian agencies CNPq-Conselho Nacional de Desenvolvimento Científico e Tecnológico (Project no. 407788/2022-0) and FINEP-Financiadora de Estudos e Projetos (Project no. 01.22.0230.00). The authors have received support from CNPq (grant number 140764/2021-6 and 382072/2023-5), and CAPES-Coordenação de Aperfeiçoamento de Pessoal de Nível Superior (grant number 88887.501183/2020-00 and 88887.374501/2019-00).

Data Availability Statement: The raw data supporting the conclusions of this article will be made available by the authors on request.

Acknowledgments: The authors would like to acknowledge UFRGS-Universidade Federal do Rio Grande do Sul for providing the infrastructure for scientific research, and the companies Globalbat and Sumesa for supplying the lithium-ion batteries.

Conflicts of Interest: The authors declare no conflict of interest.

References

1. IEA. *Global EV Outlook 2023*; IEA: Paris, France, 2023; Licence: CC BY 4.0; Available online: https://www.iea.org/reports/global-ev-outlook-2023 (accessed on 30 July 2024).
2. Yi, C.; Zhou, L.; Wu, X.; Sun, W.; Yi, L.; Yang, Y. Technology for Recycling and Regenerating Graphite from Spent Lithium-Ion Batteries. *Chin. J. Chem. Eng.* **2021**, *39*, 37–50. [CrossRef]
3. Ji, Y.; Kpodzro, E.E.; Jafvert, C.T.; Zhao, F. Direct Recycling Technologies of Cathode in Spent Lithium-Ion Batteries. *Clean Technol. Recycl.* **2021**, *1*, 124–151. [CrossRef]
4. Armand, M.; Axmann, P.; Bresser, D.; Copley, M.; Edström, K.; Ekberg, C.; Guyomard, D.; Lestriez, B.; Novák, P.; Petranikova, M.; et al. Lithium-Ion Batteries—Current State of the Art and Anticipated Developments. *J. Power Sources* **2020**, *479*, 228708. [CrossRef]
5. U.S. Geological Survey. *USGS Mineral Commodity Summaries 2023*; U.S. Geological Survey: Reston, VA, USA, 2023; Volume 210. [CrossRef]
6. Noh, H.-J.; Youn, S.; Yoon, C.S.; Sun, Y.-K. Comparison of the Structural and Electrochemical Properties of Layered Li[NixCoyMnz]O_2 (x = 1/3, 0.5, 0.6, 0.7, 0.8 and 0.85) Cathode Material for Lithium-Ion Batteries. *J. Power Sources* **2013**, *233*, 121–130. [CrossRef]
7. Bak, S.-M.; Hu, E.; Zhou, Y.; Yu, X.; Senanayake, S.D.; Cho, S.-J.; Kim, K.-B.; Chung, K.Y.; Yang, X.-Q.; Nam, K.-W. Structural Changes and Thermal Stability of Charged LiNixMnyCozO_2 Cathode Materials Studied by Combined In Situ Time-Resolved XRD and Mass Spectroscopy. *ACS Appl. Mater. Interfaces* **2014**, *6*, 22594–22601. [CrossRef]
8. Jiang, S.; Zhang, L.; Hua, H.; Liu, X.; Wu, H.; Yuan, Z. Assessment of End-of-Life Electric Vehicle Batteries in China: Future Scenarios and Economic Benefits. *Waste Manag.* **2021**, *135*, 70–78. [CrossRef]
9. Yun, L.; Linh, D.; Shui, L.; Peng, X.; Garg, A.; LE, M.L.P.; Asghari, S.; Sandoval, J. Metallurgical and Mechanical Methods for Recycling of Lithium-Ion Battery Pack for Electric Vehicles. *Resour. Conserv. Recycl.* **2018**, *136*, 198–208. [CrossRef]
10. Quan, J.; Zhao, S.; Song, D.; Wang, T.; He, W.; Li, G. Comparative Life Cycle Assessment of LFP and NCM Batteries Including the Secondary Use and Different Recycling Technologies. *Sci. Total Environ.* **2022**, *819*, 153105. [CrossRef]
11. Bharathraj, S.; Adiga, S.P.; Mayya, K.S.; Song, T.; Kim, J.; Sung, Y. Degradation-Guided Optimization of Charging Protocol for Cycle Life Enhancement of Li-Ion Batteries with Lithium Manganese Oxide-Based Cathodes. *J. Power Sources* **2020**, *474*, 228659. [CrossRef]
12. Wang, W.; Wu, Y. An Overview of Recycling and Treatment of Spent $LiFePO_4$ Batteries in China. *Resour. Conserv. Recycl.* **2017**, *127*, 233–243. [CrossRef]
13. Jiang, S.; Hua, H.; Zhang, L.; Liu, X.; Wu, H.; Yuan, Z. Environmental Impacts of Hydrometallurgical Recycling and Reusing for Manufacturing of Lithium-Ion Traction Batteries in China. *Sci. Total Environ.* **2022**, *811*, 152224. [CrossRef] [PubMed]
14. Li, P.; Luo, S.; Zhang, L.; Liu, Q.; Wang, Y.; Lin, Y.; Xu, C.; Guo, J.; Cheali, P.; Xia, X. Progress, Challenges, and Prospects of Spent Lithium-Ion Batteries Recycling: A Review. *J. Energy Chem.* **2024**, *89*, 144–171. [CrossRef]
15. Dunn, J.; Kendall, A.; Slattery, M. Electric Vehicle Lithium-Ion Battery Recycled Content Standards for the US—Targets, Costs, and Environmental Impacts. *Resour. Conserv. Recycl.* **2022**, *185*, 106488. [CrossRef]
16. Bertuol, D.A.; Toniasso, C.; Jiménez, B.M.; Meili, L.; Dotto, G.L.; Tanabe, E.H.; Aguiar, M.L. Application of Spouted Bed Elutriation in the Recycling of Lithium Ion Batteries. *J. Power Sources* **2015**, *275*, 627–632. [CrossRef]
17. Zhang, T.; He, Y.; Wang, F.; Ge, L.; Zhu, X.; Li, H. Chemical and Process Mineralogical Characterizations of Spent Lithium-Ion Batteries: An Approach by Multi-Analytical Techniques. *Waste Manag.* **2014**, *34*, 1051–1058. [CrossRef]
18. Ahuis, M.; Aluzoun, A.; Keppeler, M.; Melzig, S.; Kwade, A. Direct Recycling of Lithium-Ion Battery Production Scrap—Solvent-Based Recovery and Reuse of Anode and Cathode Coating Materials. *J. Power Sources* **2024**, *593*, 233995. [CrossRef]
19. Camargo, P.S.S.; Gomes Osório Torres, G.; Pacheco, J.A.S.; Cenci, M.P.; Kasper, A.C.; Veit, H.M. Mechanical Methods for Materials Concentration of Lithium Iron Phosphate (LFP) Cells and Product Potential Evaluation for Recycling. *Environ. Sci. Pollut. Res.* **2024**. [CrossRef]
20. Colledani, M.; Gentilini, L.; Mossali, E.; Picone, N. A Novel Mechanical Pre-Treatment Process-Chain for the Recycling of Li-Ion Batteries. *CIRP Ann.* **2023**, *72*, 17–20. [CrossRef]
21. Zhang, G.; Yuan, X.; He, Y.; Wang, H.; Zhang, T.; Xie, W. Recent Advances in Pretreating Technology for Recycling Valuable Metals from Spent Lithium-Ion Batteries. *J. Hazard. Mater.* **2021**, *406*, 124332. [CrossRef]
22. Ku, H.; Jung, Y.; Jo, M.; Park, S.; Kim, S.; Yang, D.; Rhee, K.; An, E.M.; Sohn, J.; Kwon, K. Recycling of Spent Lithium-Ion Battery Cathode Materials by Ammoniacal Leaching. *J. Hazard. Mater.* **2016**, *313*, 138–146. [CrossRef]

23. *ASTM-E473*; Terminology Relating to Thermal Analysis and Rheology. ASTM International: West Conshohocken, PA, USA, 2014; pp. 1–3.
24. *ASTM-E1131*; Test Method for Compositional Analysis by Thermogravimetry. ASTM International: West Conshohocken, PA, USA, 2015; Volume 8, p. 6.
25. Cenci, M.P.; Eidelwein, E.M.; Scarazzato, T.; Veit, H.M. Assessment of Smartphones' Components and Materials for a Recycling Perspective: Tendencies of Composition and Target Elements. *J. Mater. Cycles Waste Manag.* **2024**, *26*, 1379–1393. [CrossRef]
26. Daily Metal Prices Metal Price Charts 2024. 2024. Available online: https://www.dailymetalprice.com/ (accessed on 30 July 2024).
27. Business Analytiq Manganese Price July 2024. 2024. Available online: https://businessanalytiq.com/procurementanalytics/index/manganese-price-index/ (accessed on 30 July 2024).
28. Nuss, P.; Eckelman, M.J. Life Cycle Assessment of Metals: A Scientific Synthesis. *PLoS ONE* **2014**, *9*, e101298. [CrossRef]
29. Ortego, A.; Calvo, G.; Valero, A.; Iglesias-Émbil, M.; Valero, A.; Villacampa, M. Assessment of Strategic Raw Materials in the Automobile Sector. *Resour. Conserv. Recycl.* **2020**, *161*, 104968. [CrossRef]
30. Valero, A.; Valero, A.; Calvo, G.; Ortego, A. Material Bottlenecks in the Future Development of Green Technologies. *Renew. Sustain. Energy Rev.* **2018**, *93*, 178–200. [CrossRef]
31. Niu, B.; Xu, Z.; Xiao, J.; Qin, Y. Recycling Hazardous and Valuable Electrolyte in Spent Lithium-Ion Batteries: Urgency, Progress, Challenge, and Viable Approach. *Chem. Rev.* **2023**, *123*, 8718–8735. [CrossRef] [PubMed]
32. Miandad, R.; Rehan, M.; Barakat, M.A.; Aburiazaiza, A.S.; Khan, H.; Ismail, I.M.I.; Dhavamani, J.; Gardy, J.; Hassanpour, A.; Nizami, A.S. Catalytic Pyrolysis of Plastic Waste: Moving toward Pyrolysis Based Biorefineries. *Front. Energy Res.* **2019**, *7*, 1–17. [CrossRef]
33. Park, K.B.; Kim, J.S. Pyrolysis Products from Various Types of Plastics Using TG-FTIR at Different Reaction Temperatures. *J. Anal. Appl. Pyrolysis* **2023**, *171*, 105983. [CrossRef]
34. Slough, G. *Thermogravimetric Analysis of Powdered Graphite for Lithium-Ion Batteries*; TA Instruments: New Castle, DE, USA, 2024; pp. 1–5. Available online: https://www.tainstruments.com/applications-notes/thermogravimetric-analysis-of-powdered-graphite-for-lithium-ion-batteries/ (accessed on 2 September 2024).
35. Nazarov, V.I.; Makarenkov, D.A.; Retivov, V.M.; Popov, A.P.; Aflyatunova, G.R.; Sivachenko, L.A.; Sotnik, L.L. Features of the Pyrolysis Process of Waste Batteries Using Carbon Black as an Additive in the Construction Industry. *Constr. Mater. Prod.* **2023**, *6*, 4. [CrossRef]
36. Silveira, A.V.M.; Santana, M.P.; Tanabe, E.H.; Bertuol, D.A. Recovery of Valuable Materials from Spent Lithium Ion Batteries Using Electrostatic Separation. *Int. J. Miner. Process.* **2017**, *169*, 91–98. [CrossRef]
37. Finegan, D.P.; Cooper, S.J.; Tjaden, B.; Taiwo, O.O.; Gelb, J.; Hinds, G.; Brett, D.J.L.; Shearing, P.R. Characterising the Structural Properties of Polymer Separators for Lithium-Ion Batteries in 3D Using Phase Contrast X-Ray Microscopy. *J. Power Sources* **2016**, *333*, 184–192. [CrossRef]
38. Heidari, A.A.; Mahdavi, H. Recent Development of Polyolefin-Based Microporous Separators for Li-Ion Batteries: A Review. *Chem. Rec.* **2020**, *20*, 570–595. [CrossRef] [PubMed]
39. Gulmine, J.V.; Janissek, P.R.; Heise, H.M.; Akcelrud, L. Polyethylene Characterization by FTIR. *Polym. Test.* **2002**, *21*, 557–563. [CrossRef]
40. Signoret, C.; Edo, M.; Caro-Bretelle, A.S.; Lopez-Cuesta, J.M.; Ienny, P.; Perrin, D. MIR Spectral Characterization of Plastic to Enable Discrimination in an Industrial Recycling Context: III. Anticipating Impacts of Ageing on Identification. *Waste Manag.* **2020**, *109*, 51–64. [CrossRef] [PubMed]
41. Brogly, M.; Bistac, S.; Bindel, D. Advanced Surface FTIR Spectroscopy Analysis of Poly(Ethylene)-Block-Poly(Ethylene Oxide) Thin Film Adsorbed on Gold Substrate. *Appl. Surf. Sci.* **2022**, *603*, 154428. [CrossRef]
42. Mark Jordi FTIR for Identification of Contamination. Jordi. 2014. Available online: https://jordilabs.com/wp-content/uploads/2014/09/Case_Study_FTIR_For_Identification_Of_Contamination.pdf (accessed on 2 September 2024).
43. Martins, P.; Lopes, A.C.; Lanceros-Mendez, S. Electroactive Phases of Poly(Vinylidene Fluoride): Determination, Processing and Applications. *Prog. Polym. Sci.* **2014**, *39*, 683–706. [CrossRef]
44. Saviello, D.; Toniolo, L.; Goidanich, S.; Casadio, F. Non-Invasive Identification of Plastic Materials in Museum Collections with Portable FTIR Reflectance Spectroscopy: Reference Database and Practical Applications. *Microchem. J.* **2016**, *124*, 868–877. [CrossRef]
45. Pražanová, A.; Kočí, J.; Míka, M.H.; Pilnaj, D.; Plachý, Z.; Knap, V. Pre-Recycling Material Analysis of NMC Lithium-Ion Battery Cells from Electric Vehicles. *Crystals* **2023**, *13*, 214. [CrossRef]
46. Dadé, M.; Wallmach, T.; Laugier, O. Detailed Microparticle Analyses Providing Process Relevant Chemical and Microtextural Insights into the Black Mass. *Minerals* **2022**, *12*, 119. [CrossRef]
47. Mousa, E.; Hu, X.; Ånnhagen, L.; Ye, G.; Cornelio, A.; Fahimi, A.; Bontempi, E.; Frontera, P.; Badenhorst, C.; Santos, A.C.; et al. Characterization and Thermal Treatment of the Black Mass from Spent Lithium-Ion Batteries. *Sustainability* **2023**, *15*, 15. [CrossRef]
48. Wang, X.; Gaustad, G.; Babbitt, C.W. Targeting High Value Metals in Lithium-Ion Battery Recycling via Shredding and Size-Based Separation. *Waste Manag.* **2016**, *51*, 204–213. [CrossRef]

49. Wilke, C.; Kaas, A.; Peuker, U.A. Influence of the Cell Type on the Physical Processes of the Mechanical Recycling of Automotive Lithium-Ion Batteries. *Metals* **2023**, *13*, 1901. [CrossRef]
50. Pinegar, H.; Smith, Y.R. End-of-Life Lithium-Ion Battery Component Mechanical Liberation and Separation. *JOM* **2019**, *71*, 4447–4456. [CrossRef]
51. Wilke, C.; Kaas, A.; Peuker, U.A. Influence of the Cell Type on Yield and Composition of Black Mass Deriving from a Mechanical Recycling Process of Automotive Lithium-Ion Batteries. *Next Sustain.* **2024**, *4*, 100050. [CrossRef]
52. Blankemeyer, S.; Wiens, D.; Wiese, T.; Raatz, A.; Kara, S. Investigation of the Potential for an Automated Disassembly Process of BEV Batteries. *Procedia CIRP* **2021**, *98*, 559–564. [CrossRef]